ChemComm

COMMUNICATION

View Article Online
View Journal | View Issue

Check for updates

Cite this: *Chem. Commun.*, 2024, **60**, 1305

Received 7th September 2023,
Accepted 18th December 2023

DOI: 10.1039/d3cc04446g

rsc.li/chemcomm

Photonic Si microwell architectures for rapid antifungal susceptibility determination of *Candida auris*†

Christopher Heuer, [abc] Xin Jiang, [a] Gali Ron,[a] Orna Ternyak,[d] Thomas Scheper,[b] Janina Bahnemann [c] and Ester Segal [*a]

We present the application of a photonic silicon chip-based optical sensor system for expeditious and phenotypic antifungal susceptibility testing. This label-free diagnostic assay optically monitors the growth of *Candida auris* at varying antifungal concentrations on a microwell-structured silicon chip in real-time, and antifungal susceptibility is detected within 6 h, four times faster than in the current gold standard method.

In recent years, multidrug-resistant fungal pathogens have emerged as a global health threat, with high mortality rates resulting in over 1.6 million deaths annually.[1,2] The severity of this situation is underscored by the World Health Organization's first-ever fungal priority pathogens list published in 2022, aiming to guide public health strategies against pathogenic fungi.[3] The excessive use of antifungals, together with climate change, accelerates the emergence and evolution of resistant fungal pathogens.[4,5] The spread of fungal infections in the last three years is mainly ascribed to the increasing number of immunocompromised and vulnerable patients,[3] which is closely linked to the COVID-19 pandemic.[6] The yeast *Candida auris* (*C. auris*), well known for its pathogenicity and associated morbidity, is now classified as an urgent threat by the United States Centers for Disease Control and Prevention.[7] *C. auris* is not only difficult to eradicate from clinical settings but is often multidrug-resistant, with some isolates being recognized as pan-resistant (resistant to antifungals of all drug classes).[3,8] Thus, there is a paramount need for diagnostic methods that can expeditiously determine the correct antifungal prescription, improving therapy outcomes and minimizing the spread of resistance.[9] Specifically, antifungal susceptibility testing (AFST), in which pathogenic fungi are exposed to varying antifungals at increasing concentrations, and the minimum inhibitory concentration (MIC) is determined, can help physicians to guide treatment decisions.[10] However, current AFST methods, like agar-based tests or the gold standard broth microdilution (BMD), are lengthy and require >24 h.[10] Also, commercially available state-of-the-art automated methods such as the Vitek2 (bioMérieux) typically provide results only within 12–18 h,[11,12] a limited set of antifungals is available, and MIC values have not always been accurately determined.[13] Thus, there is an urgent clinical need for rapid and reliable novel AFST methods for *Candida* species.

Herein, we present the use of a photonic silicon chip with microwell diffraction gratings that serves as a sensitive sensor for label-free fungal growth monitoring by detecting changes in white light reflectance. Such silicon-based materials are characterized by their biocompatibility and have been widely employed for diagnostic, therapeutic and biosensing applications.[14–16] Specifically, we have previously shown that photonic silicon chips, with different dimensions and microtopologies,[17] can be used for rapid susceptibility testing of the bacterial species *Escherichia coli* (*E. coli*) within 90 minutes[18–20] and the mould *Aspergillus niger* (*A. niger*) within 10–12 h[21] using phase-shift reflectometric interference spectroscopic measurements (PRISM) and intensity-based PRISM (iPRISM) tests. In these optical assays, the photonic silicon chips are individually fixated into heat-controlled microfluidic channels, and suspensions of yeast cells in growth medium are introduced into these channels (see Fig. 1A). The chips consist of arrays of microwells (width: ~4 μm and depth: ~4 μm) that were specifically designed to fit the majority of *C. auris* cells (having spherical to oval shape with characteristic dimensions of 2–3 × 2.5–5 μm[22]) within the individual wells, see Fig. 1B-i for cross-section and top view (insert) scanning electron microscopy (SEM) images. Yet, *C. auris* can also form cell aggregates which are mainly found on top of the microwells. Continuous reflectance measurements are used to obtain characteristic spectra (Fig. 1B-ii), which are further processed by Fast Fourier

[a] *Department of Biotechnology and Food Engineering, Technion – Israel Institute of Technology, Haifa, 3200003, Israel. E-mail: esegal@technion.ac.il*
[b] *Institute of Technical Chemistry, Leibniz University Hannover, Hannover 30167, Germany*
[c] *Institute of Physics, University of Augsburg, Augsburg 86159, Germany*
[d] *Micro- and Nanofabrication and Printing Unit, Technion – Israel Institute of Technology, Haifa, 3200003, Israel*

† Electronic supplementary information (ESI) available. See DOI: https://doi.org/10.1039/d3cc04446g

Open Access Article. Published on 27 décembre 2023. Downloaded on 2026-05-14 15:42:59.
This article is licensed under a Creative Commons Attribution-NonCommercial 3.0 Unported Licence.

Open Access Article. Published on 27 décembre 2023. Downloaded on 2026-05-14 15:42:59.
This article is licensed under a Creative Commons Attribution-NonCommercial 3.0 Unported Licence.

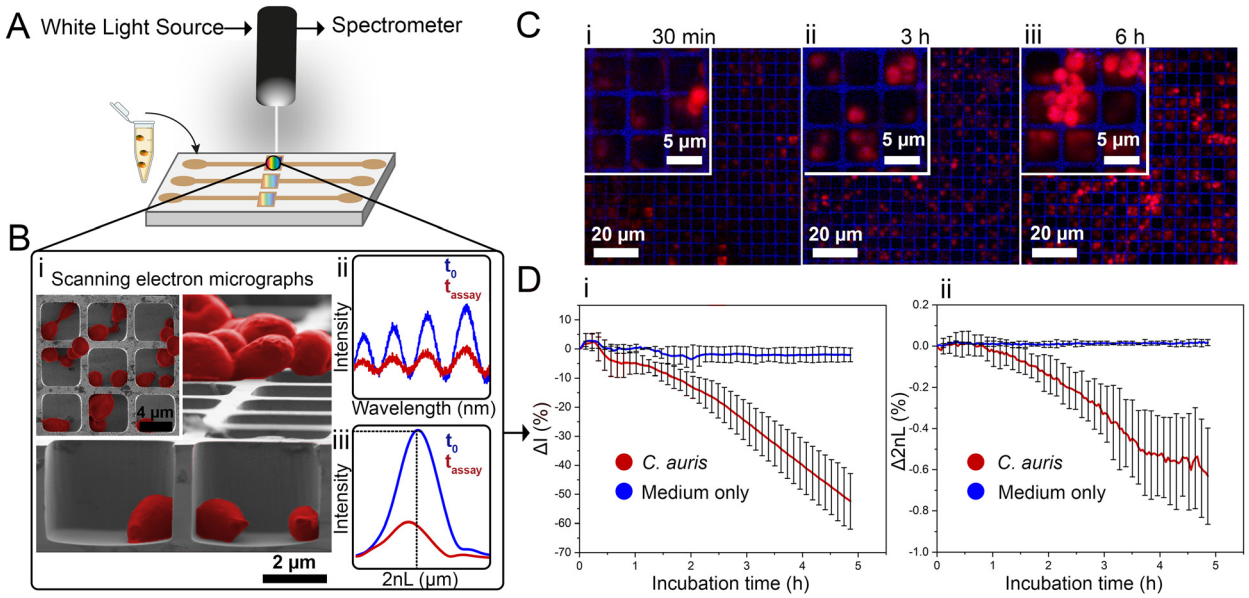

Fig. 1 iPRISM concept for *C. auris* growth monitoring. (A) Suspensions of *C. auris* cells in growth medium (RPMI) are introduced onto a photonic silicon chip, having a periodic microwell array structure, fixated within microfluidic channels (channels height ~ 1 mm allowing for cells suspensions, growth medium and antifungal solution to flow on top of the microwells). The chip microstructure is specifically designed to (B-i) accommodate *C. auris* cells within the microwells as demonstrated by top view and cross section (insert) SEM micrographs. Cells are false-coloured in red for clarity. A white light source is positioned normal to the chips and illuminates the sensor elements, while the reflected light is continuously recorded. (B-ii) The resulting reflectance spectra show characteristic interference fringes, as the incident light is reflected from the top and bottom interfaces of the microwell arrays. The latter spectra are recorded and transformed into (B-iii) single peaks by frequency analysis. The amplitude of the peak corresponds to the intensity of the reflected light and the peak position correlates to the 2*nL*. (C) Confocal laser scanning microscopy after cell staining with propidium iodide reveals *C. auris* cells (initial cell density: McFarland 2.0) growing within and on top of the silicon microstructure resulting in characteristic growth curves with a continuous averaged (n = 3) decrease of the (D-i) intensity and (D-ii) 2*nL* signals. Error bars depict standard deviations.

Transform (FFT) frequency analysis. The latter results in a single peak (Fig. 1B-iii), where the peak amplitude corresponds to the intensity of the reflected light and the peak position corresponds to 2*nL* (n refers to the refractive index of a medium within the grating and L is the microwells' depth). Please also refer to Fig. S1 (ESI†) and to our previous works[19,23,24] for a detailed explanation of the involved optical principles.

Monitoring both parameters over time allows tracking *C. auris* growth in a label-free manner in real-time. Fig. 1D depicts growth curves (intensity and 2*nL*) for *C. auris* suspensions at McFarland value of 2.0 (which corresponds to $\sim 10^7$ cells mL^{-1}, as routinely used for AFST of *Candida* species by commercial automated systems such as the Vitek2;[12] for experimental details and further discussion on *C. auris* cell density see the ESI,† Fig. S2). For both parameters, a general trend of decreasing signals (intensity slope: $-10.8\ \Delta I$ (%) h^{-1} and 2*nL* slope: $-0.13\ \Delta 2nL$ (%) h^{-1}) is observed (see Fig. 1D-i and ii). The major decrease in the intensity signal is ascribed to *C. auris* cells growing on the microstructured silicon surface[19,23] and Fig. S3 (ESI†) depicts the correlation between cell concentrations and the obtained intensity signal (Fig. S4 (ESI†) presents the corresponding raw reflectance spectra). Fig. 1C shows corresponding confocal laser scanning micrographs of *C. auris* at different time points (30 min, 3 h, 6 h), demonstrating that at the beginning of the assay, most cells reside within the microwells. Whereas at later times, the cells tend to grow out of the wells and are found on the top of the microstructure, as also revealed by SEM studies presented in Fig. S5 (ESI†). Moreover, similar behaviour is also observed for a second yeast species – the industrial-relevant *Saccharomyces cerevisiae* where a characteristic reduction in both intensity and 2*nL* signals is obtained, see Fig. S6 (ESI†).

While the observed intensity decrease is in agreement with our previous studies, where varying microorganisms were grown on microstructured silicon gratings,[17,19,21] the obtained trend of 2*nL* reduction (Fig. 1D-ii) is different from the typical behaviour we have observed for bacteria.[19,21] In general, we found that bacterial cells tend to reside and proliferate within the microwell structure (see Fig. S7, ESI†) and, as such, induce an increase in the 2*nL* value over time. The latter is ascribed to an increase in the average refractive index within the microstructure.[17–19] We were expecting a similar behaviour for *C. auris*, as most cells are found to reside in the wells at the beginning of the assay. Yet, within 6 h *C. auris* forms dense cell aggregates on the top of the microstructure, as depicted in the electron micrographs included in Fig. S5 (ESI†). To further investigate this behaviour, *C. auris* was studied in a growth medium designated for bacteria (CAMHB), where growth is observed to be impaired compared to that in RPMI (designated for yeasts). The slope of the intensity signal is found to be five times lower in CAMHB, while the 2*nL* slope is mainly unchanged, see Fig. S8 (ESI†). Moreover, SEM studies show that *C. auris* do not form aggregates on top of the silicon microstructure in CAMHB, as also depicted in Fig. S8 (ESI†).

 This journal is © The Royal Society of Chemistry 2024

Open Access Article. Published on 27 décembre 2023. Downloaded on 2026-05-14 15:42:59.
This article is licensed under a Creative Commons Attribution-NonCommercial 3.0 Unported Licence.

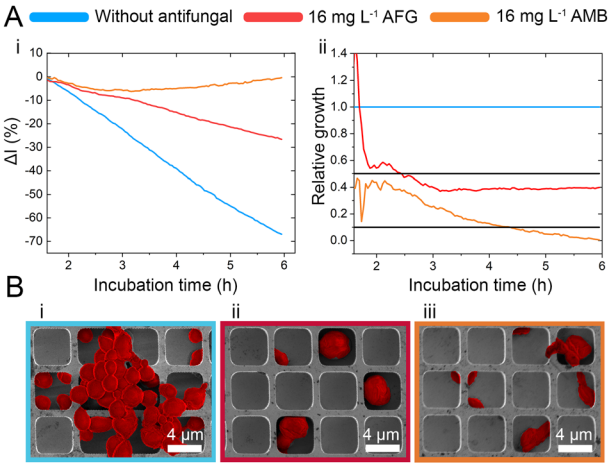

Fig. 2 iPRISM "overkill" experiments. (A-i) iPRISM growth curves for unhindered growth and *C. auris* exposed to 16 mg L^{-1} anidulafungin (AFG) and amphotericin B (AMB), respectively. These growth curves are transformed into relative growth where the unhindered growth is defined as 100% (1.0) growth. Black threshold lines indicate 50% (0.5) and 10% (0.1) growth. (B-i to B-iii) Scanning electron microscopy images reveal how *C. auris* behaves on the microstructure in the absence and presence of high antifungal concentrations. Cells are false-coloured in red for clarity.

This may suggest that the cells emerging from the wells and forming dense cell clusters on the top of the microstructure potentially impede light interference from the chip, resulting in a reduction of the *2nL* signal. However, this phenomenon should be further investigated as we also observed it in the case of biofilm formation by the bacterial pathogen *Pseudomonas aeruginosa*.[17] Herein, we will mainly focus on monitoring the intensity changes for sensitive growth detection at varying antifungal concentrations, following the iPRISM assay principle.[21] The iPRISM concept for AFST of *C. auris* was first established with high antibiotic concentrations (see Fig. 2) of two clinically relevant antifungal agents with different modes of action, namely anidulafungin (echinocandin: inhibition of cell wall biosynthesis)[25] and amphotericin B (polyene: cell membrane damage).[26,27] The tested concentrations of these drugs (both 16 mg L^{-1}) are at the upper range of the recommended concentrations for AFST of *Candida* species according to BMD protocols by the European Society of Antimicrobial Susceptibility Testing (EUCAST).[28] Thus, fungal growth is inhibited at these concentrations (Fig. 2A-i), and the relative growth compared to the drug-free control falls below the 50% (anidulafungin) and 10% (amphotericin B) growth values, as depicted in Fig. 2A-ii. The latter values also serve as the MIC threshold for these respective antifungals (anidulafungin MIC: lowest drug concentration with $\geq$50% growth inhibition and amphotericin B MIC: lowest drug concentration with $\geq$90% growth inhibition) according to EUCAST.[28] Scanning electron micrographs (Fig. 2Bi–iii) reveal that in the absence of an antifungal drug, *C. auris* grow in dense networks within and on top of the silicon microstructure, while when exposed to an antifungal, fewer cells are observed on the chip surface (Fig. 2B-ii and iii). Moreover, cells exposed to anidulafungin (Fig. 2B-ii) appear round and swollen – characteristic of morphological changes induced by this type of antifungal agent.[29] In the case of amphotericin B, cells exhibit a deformed appearance, which is ascribed to cell membrane damage (Fig. 2B-iii).[30]

C. auris cells were grown at various concentrations of anidulafungin and amphotericin B in order to determine MIC values, and Fig. 3 depicts the corresponding relative growth curves. Increased concentrations of both antifungal agents result in reduced growth compared to the untreated control. According to the MIC definitions (as explained above), the iPRISM MIC values are 0.25 mg L^{-1} for both drugs. Statistical analysis of iPRISM results obtained from different chips (as shown in Fig. S9, ESI†) reveals that MIC value determination is feasible within 3.5 h and 6 h for anidulafungin and amphotericin B, respectively. Thus, the iPRISM platform provides a significantly reduced assay time compared to the gold-standard BMD (time: 24 h) and the commercially available Vitek2 system (time: 12–18 h).[11,12,28] Please also refer to Fig. S11 (ESI†), demonstrating that standard BMD-based MIC

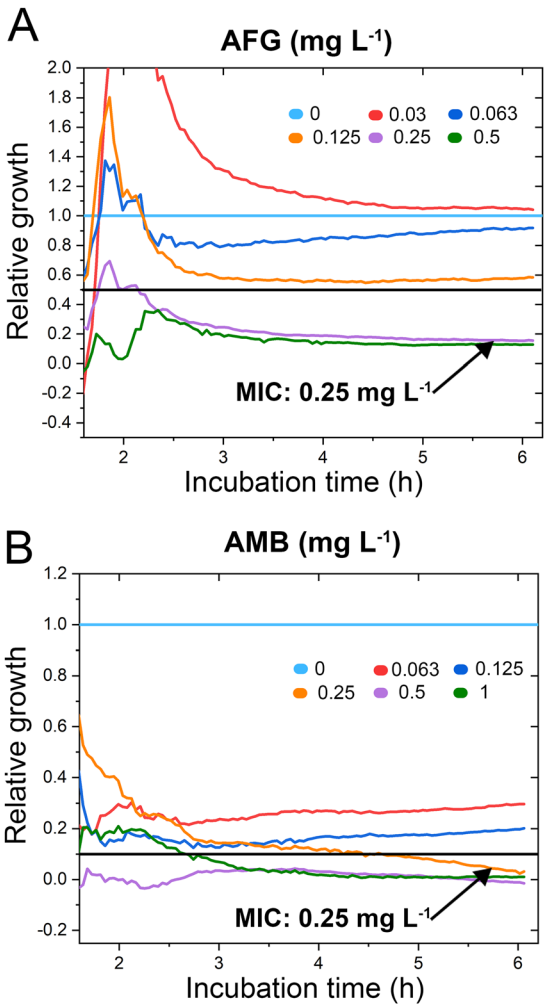

Fig. 3 *C. auris* iPRISM AFST. Relative growth of *C. auris* at varying concentrations of (A) anidulafungin (AFG) and (B) amphotericin B (AMB). The underlying intensity changes and also the corresponding *2nL* growth curves are presented in Fig. S10 (ESI†), demonstrating that the intensity is superior in its quantitative sensitivity for growth at varying antifungal concentrations while the *2nL* is still sensitive qualitatively.

Open Access Article. Published on 27 décembre 2023. Downloaded on 2026-05-14 15:42:59.
This article is licensed under a Creative Commons Attribution-NonCommercial 3.0 Unported Licence.

value determination (*C. auris* and amphotericin B) can be reduced to 19 h using continuous microplate reader measurements and statistical analysis. Thus, the presented iPRISM assay still provides a significantly faster MIC determination.

To test the accuracy of the obtained MIC values, we compare the latter concentrations to the outcome of gold standard BMD performed according to EUCAST protocols, see Table S1 in the ESI.† The iPRISM MIC values for anidulafungin (0.25 mg L^{-1} *vs.* 0.0625 mg L^{-1}) and amphotericin B (0.25 mg L^{-1} *vs.* 0.125–0.25 mg L^{-1}) are one to two dilutions higher than the BMD value. Such a difference between two dilutions is considered as an essential agreement.[31] Furthermore, the obtained MIC values do not exceed the tentative epidemiological cut-off values (ECOFFs) determined by different approaches (Table S1, ESI†).[32] As such, for both drugs, this *C. auris* isolate is correctly classified into the wild-type population without acquired drug resistance. It should be noted that MIC value deviations between different methods and protocols are often encountered in susceptibility testing.[33] As previously observed, MIC values determined by (i)PRISM for *E. coli*[18,19] and *A. niger*[21] tend to be higher in comparison to BMD MICs. These deviations are mainly ascribed to the different assay procedures. While in the BMD, the fungal cells are suspended and grow in a liquid medium, in the iPRISM assay, the behaviour of the cell-silicon substrate interface is monitored.

A diagnostic platform for rapid and phenotypic AFST of *C. auris* as a model yeast pathogen is shown, demonstrating and extending the applicability of this label-free assay to a wide variety of clinically relevant species (bacteria, filamentous fungi, yeast). The yeast cells grow on a microstructured silicon surface that also serves as a sensitive sensing element allowing the detection of changes in the white light reflectivity. The latter changes are correlated to fungal growth and used to study the behaviour of *C. auris* upon exposure to anidulafungin and amphotericin B – two clinically relevant antifungals from two distinct antifungal classes. MIC values for these antifungals can be obtained within 6 h and agree with values determined by classical BMD. Thus, iPRISM provides a novel method for AFST of *Candida* species that is significantly faster (time reduction: $\geq$18 h) than gold standard methods.

This work was supported by the Israel Science Foundation (grant No. 2458/21). We also acknowledge funding by the German Research Foundation (DFG) *via* the Emmy Noether program (project ID346772917), and grant SCHE 279/32-2, as well as by the VolkswagenStiftung *via* the program ''Niedersächsisches Vorab: Research Cooperation Lower Saxony—Israel''. The authors thank the staff of the Micro- and Nanofabrication and Printing Unit (MNFPU) at the Technion for the fabrication of the photonic silicon chips.

Conflicts of interest

There are no conflicts to declare.

References

1 K. Benedict, M. Richardson, S. Vallabhaneni, B. R. Jackson and T. Chiller, *Lancet Infect. Dis.*, 2017, **17**, e403–e411.
2 A. Rokas, *Nat. Microbiol.*, 2022, **7**, 607–619.
3 WHO fungal priority pathogens list to guide research, development and public health action, **https://www.who.int/publications/i/item/978924006024**, (accessed March 2023).
4 U. Hofer, *Nat. Rev. Microbiol.*, 2019, **17**, 588.
5 N. A. R. Gow, C. Johnson, J. Berman, A. T. Coste, C. A. Cuomo, D. S. Perlin, T. Bicanic, T. S. Harrison, N. Wiederhold, M. Bromley, T. Chiller and K. Edgar, *Nat. Commun.*, 2022, **13**, 5352.
6 CDC special report 2022: COVID-19 U.S. impact on antimicrobial resistance.
7 CDC report: antibiotic resistance threats in the United States 2019.
8 B. O'Brien, J. Liang, S. Chaturvedi, J. L. Jacobs and V. Chaturvedi, *Lancet Microbe*, 2020, **1**, e193–e194.
9 D. S. Perlin, R. Rautemaa-Richardson and A. Alastruey-Izquierdo, *Lancet Infect. Dis.*, 2017, **17**, e383–e392.
10 C. Heuer, J. Bahnemann, T. Scheper and E. Segal, *Small methods*, 2021, **5**, 2100713.
11 M. Cuenca-Estrella, A. Gomez-Lopez, A. Alastruey-Izquierdo, L. Bernal-Martinez, I. Cuesta, M. J. Buitrago and J. L. Rodriguez-Tudela, *J. Clin. Microbiol.*, 2010, **48**, 1782.
12 E. Borghi, R. Iatta, R. Sciota, C. Biassoni, T. Cuna, M. T. Montagna and G. Morace, *J. Clin. Microbiol.*, 2010, **48**, 3153–3157.
13 S. Kathuria, P. K. Singh, C. Sharma, A. Prakash, A. Masih, A. Kumar, J. F. Meis and A. Chowdhary, *J. Clin. Microbiol.*, 2015, **53**, 1823–1830.
14 Y. Chen, M. Alba, T. Tieu, Z. Tong, R. Singh Minhas, D. Rudd, N. H. Voelcker, A. Cifuentes-Rius and R. Elnathan, *Adv. NanoBiomed Res.*, 2021, **1**, 2100002.
15 T. Tieu, M. Alba, R. Elnathan, A. Cifuentes-Rius and N. H. Voelcker, *Adv. Ther.*, 2018, **2**, 1800095.
16 C. Pacholski, *Sensors*, 2013, **13**, 4694–4713.
17 H. Leonard, X. Jiang, S. Arshavsky-Graham, L. Holtzman, Y. Haimov, D. Weizman, S. Halachmi and E. Segal, *Nanoscale Horiz.*, 2022, **7**, 729–742.
18 C. Heuer, J.-A. Preuss, M. Buttkewitz, T. Scheper, E. Segal and J. Bahnemann, *Lab Chip*, 2022, **22**, 4950–4961.
19 H. Leonard, S. Halachmi, N. Ben-Dov, O. Nativ and E. Segal, *ACS Nano*, 2017, **11**, 6167–6177.
20 X. Jiang, T. Borkum, S. Shprits, J. Boen, S. Arshavsky-Graham, B. Rofman, M. Strauss, R. Colodner, J. Sulam, S. Halachmi, H. Leonard and E. Segal, *Adv. Sci.*, 2023, e2303285.
21 C. Heuer, H. Leonard, N. Nitzan, A. Lavy-Alperovitch, N. Massad-Ivanir, T. Scheper and E. Segal, *ACS Infect. Dis.*, 2020, **6**, 2560–2566.
22 J. Osei Sekyere, *MicrobiologyOpen*, 2018, **7**, e00578.
23 Y. Mirsky, A. Nahor, E. Edrei, N. Massad-Ivanir, L. M. Bonanno-Young, E. Segal and A. Sa'ar, *Appl. Phys. Lett.*, 2013, **103**, 033702.
24 N. Massad-Ivanir, Y. Mirsky, A. Nahor, E. Edrei, L. M. Bonanno-Young, N. Ben Dor, A. Sa'ar and E. Segal, *Analyst*, 2014, **139**, 3885–3894.
25 J. A. Vazquez and J. D. Sobel, *Clin. Infect. Dis.*, 2006, **43**, 215.
26 A. Zumbuehl, D. Jeannerat, S. E. Martin, M. Sohrmann, P. Stano, T. Vigassy, D. D. Clark, S. L. Hussey, M. Peter, B. R. Peterson, E. Pretsch, P. Walde and E. M. Carreira, *Angew. Chem.*, 2004, **116**, 5293–5297.
27 S. L. Regen, *JACS Au*, 2021, **1**, 3–7.
28 EUCAST DEFINITIVE DOCUMENT E.DEF 7.3.2 Method for the determination of broth dilution minimum inhibitory concentrations of antifungal agents for yeasts.
29 N. Yagüe, L. Gómez-Delgado, M. Á. Curto, V. S. D. Carvalho, M. B. Moreno, P. Pérez, J. C. Ribas and J. C. G. Cortés, *Pharmaceuticals*, 2021, **14**, 1332.
30 E. Grela, A. Zdybicka-Barabas, B. Pawlikowska-Pawlega, M. Cytrynska, M. Wlodarczyk, W. Grudzinski, R. Luchowski and W. I. Gruszecki, *Sci. Rep.*, 2019, **9**, 17029.
31 N. P. Wiederhold, *Open Forum Infect. Dis.*, 2021, **8**, ofab444.
32 M. C. Arendrup, A. Prakash, J. Meletiadis, C. Sharma and A. Chowdhary, *Antimicrob. Agents Chemother.*, 2017, **61**, e00485-17.
33 C. B. Terwee, L. D. Roorda, J. Dekker, S. M. Bierma-Zeinstra, G. Peat, K. P. Jordan, P. Croft and H. C. W. de Vet, *J. Clin. Epidemiol.*, 2010, **63**, 524–534.

 This journal is © The Royal Society of Chemistry 2024